Proceedings of *RAGtime ?/?: Workshops on black holes and neutron stars*
S. Hledík and Z. Stuchlík, editors, Silesian University in Opava, Czech Republic, ????, pp. 1–15

Variation of the primary and reprocessed radiation in the flare–spot model

Michal Dovčiak[1,a] Vladimír Karas[1] Giorgio Matt[2] and René W. Goosmann[1]

[1]Astronomical Institute, Academy of Sciences of the Czech Republic, Boční II, CZ-140 31 Prague, Czech Republic
[2]Dipartimento di Fisica, Università degli Studi "Roma Tre", Via della Vasca Navale 84, I-00146 Roma, Italy
[a]dovciak@astro.cas.cz

ABSTRACT
We study light curves and spectra (equivalent widths of the iron line and some other spectral characteristics) which arise by reprocessing on the surface of an accretion disc, following its illumination by a primary off-axis source — an X-ray 'flare', assumed to be a point-like source just above the accretion disc. We consider all general relativity effects (energy shifts, light bending, time delays, delay amplification due to the spot motion) near a rotating black hole. For some sets of parameters the reflected flux exceeds the flux from the primary component. We show that the orbit-induced variations of the equivalent width with respect to its mean value can be as high as 30% for an observer's inclination of 30°, and much more at higher inclinations. We calculate the ratio of the reflected flux to the primary flux and the hardness ratio which we find to vary significantly with the spot phase mainly for small orbital radii. This offers the chance to estimate the lower limit of the black hole spin if the flare arises close to the black hole. We show the results for different values of the flare orbital radius.

Keywords: line: profiles – relativity – galaxies: active – X-rays: galaxies

1 INTRODUCTION

X-ray spectral measurements of the iron line and the underlying continuum provide a powerful tool to study accretion discs in active galactic nuclei (AGN) and Galactic black holes, for a review see Fabian et al. (2000); Reynolds and Nowak (2003). If a line originates by reflection of the primary continuum, then its observed characteristics may reveal rapid orbital motion and light bending near the central black hole. Spectral characteristics can be employed to constrain the black hole mass and angular momentum. A particularly important role is played by the equivalent width (EW), which reflects the intensity of the line versus the continuum flux as

well as the role of general relativity effects in the source. In order to reduce the ambiguity of the results one needs to perform spectral fitting with self-consistent models of both the line and continuum.

Some AGN are known to exhibit iron lines with an EW greater than expected for a "classical" accretion disc. Enhanced values for the EW can be obtained by assuming an anisotropical distribution of the primary X-rays (Ghisellini et al., 1991), significant ionization of the disc matter (Matt et al., 1993) or iron overabundance (George and Fabian, 1991). Martocchia and Matt (1996) and Martocchia et al. (2000) found, using an axisymmetric lamp-post scheme, an anticorrelation between the intensity of the reflection features and the primary flux. When the primary source is at a low height on the disc axis, the EW can be increased by up to an order of magnitude with respect to calculations neglecting general relativity effects. When allowing the source to be located off the axis of rotation, an even stronger enhancement is expected (Dabrowski and Lasenby, 2001). Miniutti et al. (2003) and Miniutti and Fabian (2004) have realised that this so-called light bending model can naturally explain the puzzling behaviour of the iron line of MCG–6-30-15, when the line saturates at a certain flux level and then its EW starts decreasing as the continuum flux increases further. Niedzwiecki and Zycki (2007) point out that the illumination by radiation which returns to the disc (following the previous reflection of the primary emission) also contributes significantly to the formation of the line profile in some cases. This results into the line profile with a pronounced blue peak unless the reflecting material is absent within the innermost 2–3 gravitational radii.

In our previous paper (Dovčiak, 2004), we have proposed that the orbiting spot model could explain the origin of transient narrow lines, which have been reported in some AGN X-ray spectra (Turner et al., 2002; Guainazzi, 2003; Yaqoob et al., 2003) and widely discussed since then. The main purpose of the current paper is to present accurate computations of time-dependent EWs and other spectral characteristics within the framework of the flare-spot model, taking into account a consistent scheme for the local spectrum reprocessing. The main difference from previous papers is that the current one combines the primary source power-law continuum with the reprocessed spectral features. Both components are further modified by relativistic effects as the signal propagates towards an observer.

In a parallel paper, Dovčiak et al. (2007), we study general relativistic effects and spectral characteristics (EWs, hardness ratio, etc.) for the flare-spot model in two model setups — the Schwarzschild black hole with a flare arising at radius $7\,r_{\rm g}$ and an extremally rotating black hole with a flare at $3\,r_{\rm g}$. In the current paper we would like to present the results of our computations for more values of the flare orbital radius. We also show that for a given flare radius the resultant spectra do not differ much for different spins of the black hole.

In Section 2 we describe the model and the approximation used and in Section 3 we present the results of our calculations. For a more detailed description of the model and for the equations used we refer the reader to the paper Dovčiak et al. (2007).

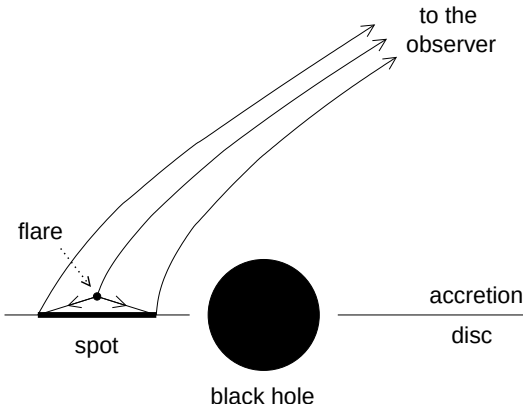

Figure 1. A sketch of the model geometry (not to scale). A localized flare occurs above the disc, possibly due to magnetic reconnection, and creates a spot by illuminating the disc surface. The resulting 'hot spot' co-rotates with the disc and contributes to the final observed signal by reprocessing the primary X-rays.

2 MODEL APPROXIMATIONS AND LIMITATIONS

We examine a system composed by a black hole, an accretion disc and a co-rotating flare with the spot underneath (Collin et al., 2003), see Fig. 1. The gravitational field is described in terms of the Kerr metric (Misner et al., 1973). Both static Schwarzschild and rotating Kerr black holes are considered. The co-rotating Keplerian accretion disc is geometrically thin and optically thick, therefore we take into account only photons coming from the equatorial plane directly to the observer. We further assume that the matter in the accretion disc is cold and neutral.

A flare is supposed to arise in the disc corona due to a magnetic reconnection event (Galeev et al., 1979; Poutanen and Fabian, 1999; Merloni and Fabian, 2001). Details of the formation of the flare and its structure are not the subject of the present paper, instead we assume that the flare is an isotropic stationary point source with a power-law spectrum, located very near above the disc. It co-rotates with the accretion disc. We also assume that a single flare dominates the intrinsic emission for a certain period of time.

The spot represents the flare-illuminated part of the disc surface. We consider the spot to be a rigid two dimensional circular feature, with its centre directly below the flare. Thus the spot does not share the differential rotation with the disc material. However, the matter in the disc lit by the flare is in Keplerian motion at the corresponding radii, and so it has different velocities at different parts of the spot (which is important when calculating the transfer function for the observer in the infinity). Because the flare is very close to the disc, the spot does not extend far from below the flare. We approximate the photon trajectories between the flare and the spot by straight lines and we do not consider the energy shift and abberation

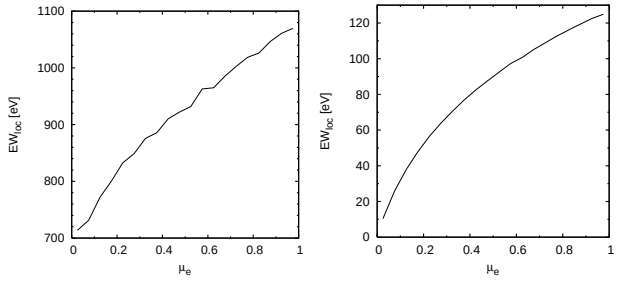

Figure 2. Left: The local equivalent width without taking the primary flux into account as a function of the direction of emission. **Right:** The same as in the left panel but with the flux from the primary source included.

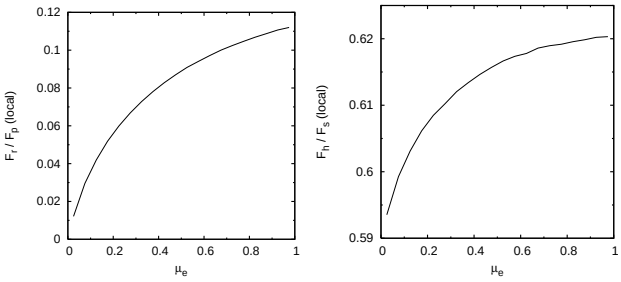

Figure 3. Left: The ratio of the locally emitted energy flux in the direction μ_e to the primary flux. The fluxes are integrated in the energy range 3–10 keV. **Right:** The local hardness ratio of the fluxes in the ranges 6.5–10 keV (F_h) and 3–6.5 keV (F_s).

due to the different motion of the flare and matter illuminated by it. Furthermore we neglect the time delay between the photon's emission from the flare and its later re-emission from the spot.

The intrinsic (local) spectra from the spot were computed by Monte Carlo simulations considering multiple Compton scattering and iron line fluorescence in a cold, neutral, constant density slab with solar iron abundance. We used the NOAR code for these computations, see Section 5 of Dumont et al. (2000) and Chapter 5 of Goosmann (2006). The local flux depends on the local incident and local emission angles, hence the flux changes across the spot. Here and elsewhere in the text we refer to the quantities measured in the local frame co-moving with the matter in the disc as "local".

The local flux consists of only two components — the flux from the primary source (the flare) and the reflected flux from the spot. The latter one consists of the reflection continuum (with the Compton hump and the iron edge as the main features) and the neutral Kα and Kβ iron lines. No other emission is taken into

account. The spectral properties of the local emission (the local EW, ratio of the reflected flux to the primary one and hardness ratio) are shown in Figs. 2 and 3.

As far as the photon trajectories from the spot to the observer are concerned, all general relativistic effects — energy shift, aberration, light bending, lensing and relative time delays — are taken into account. We assume that only the gravity of the central black hole influences the photons on their path from the disc to the observer. This allows us to define a relatively simple scheme in which different intervening effects remain under full control and can be well identified.

3 SPECTRAL CHARACTERISTICS OF THE OBSERVED SIGNAL

The observed light curves computed for the spot in the vicinity of the extremally spinning Kerr black hole ($a = 0.998\,GM/c^3$) and the Schwarzschild black hole ($a = 0\,GM/c^3$) in the 3–10 keV energy range for different orbital radius can be seen in Figs. 4 and 5. The light curves are influenced mainly by the overall amplification factor, transfer function and delay amplification [see paper (Dovčiak et al., 2007) for details], and by the dependence of the local flux on the emission angle. The primary emission dominates the observed flux as expected, meanwhile the reflected flux in the Fe lines from the spot contributes less. There is an exception in this behaviour, though, for some parts of the orbit close to the black hole (see top row of Fig. 4). The reflected flux from the spot exceeds the flux of the primary for the orbital radius $r = 3\,GM/c^2$ and for the inclinations $\theta_\mathrm{o} = 60°$ and 85°. The variations of the flux decrease with the orbital radius as expected. Note, that the amplification of the emission due to the lensing effect is still relevant as far as $100\,GM/c^2$ for large inclination angles (85°).

Figs. 6 and 7 shows the mean spectra taken over the whole orbit. The line is smeared when taken over the whole orbit. As it is well known (Iwasawa et al., 1996) in the Schwarzschild case, if we assume that the emission comes mainly from above the innermost stable orbit, the line stays above 3 keV, while in the Kerr case it can be shifted even below this energy (as is the case for all shown inclinations for the spot orbit below $4\,GM/c^2$). The iron edge is smeared in all studied cases and the dominance of the primary emission is evident. As we expect, the line is less shifted with the increasing orbital radius but it is still substantially broadened even at the radius $100\,GM/c^2$ due to the large orbital velocity of the spot.

In order to quantify the properties of the observed spectra let us look at the equivalent width, ratio of the observed reflected and primary components, and the hardness ratio (Figs. 8 and 9).

A closer look at the EW, see the left panels in Figs. 8 and 9, reveals that it does not much differ from its local value (Fig. 2), i.e. $EW(t) \approx EW_\mathrm{loc}(\mu_\mathrm{e}(t))$ (for the dependence $\mu_\mathrm{e}(t)$ for some radii see Dovčiak et al. (2007)). This is not, however, true for the case of the low orbital radius with an observer inclination of 85° when the EW is magnified due to the lensing effect. For the spot close to the black hole ($r = 3\,GM/c^2$) the EW is changing with respect to its mean value by 30% even for a low inclination angle 30°. For an almost edge-on disc it can vary by as much

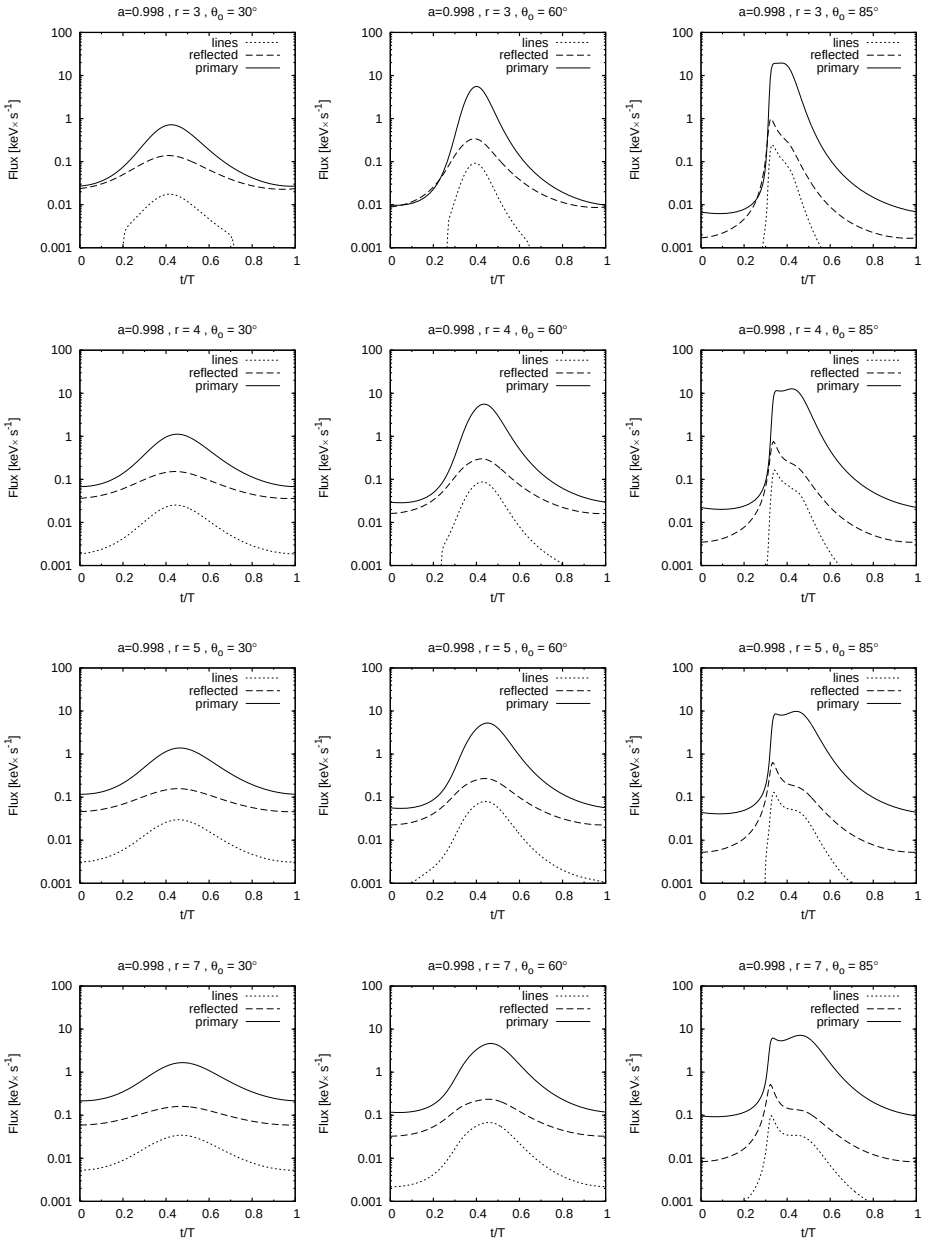

Figure 4. The light curves of the observed emission from the flare and the spot for the energy range 3–10 keV for the Kerr black hole with the spin $0.998\,GM/c^3$, the spot orbital radii 3, 4, 5 and 7 GM/c^2 (from top to bottom) and the observer's inclination angles 30°, 60° and 85° (from left to right). The primary emission, spot's continuum emission and spot's emission in Kα and Kβ lines are denoted by solid, dashed and dotted graphs, respectively.

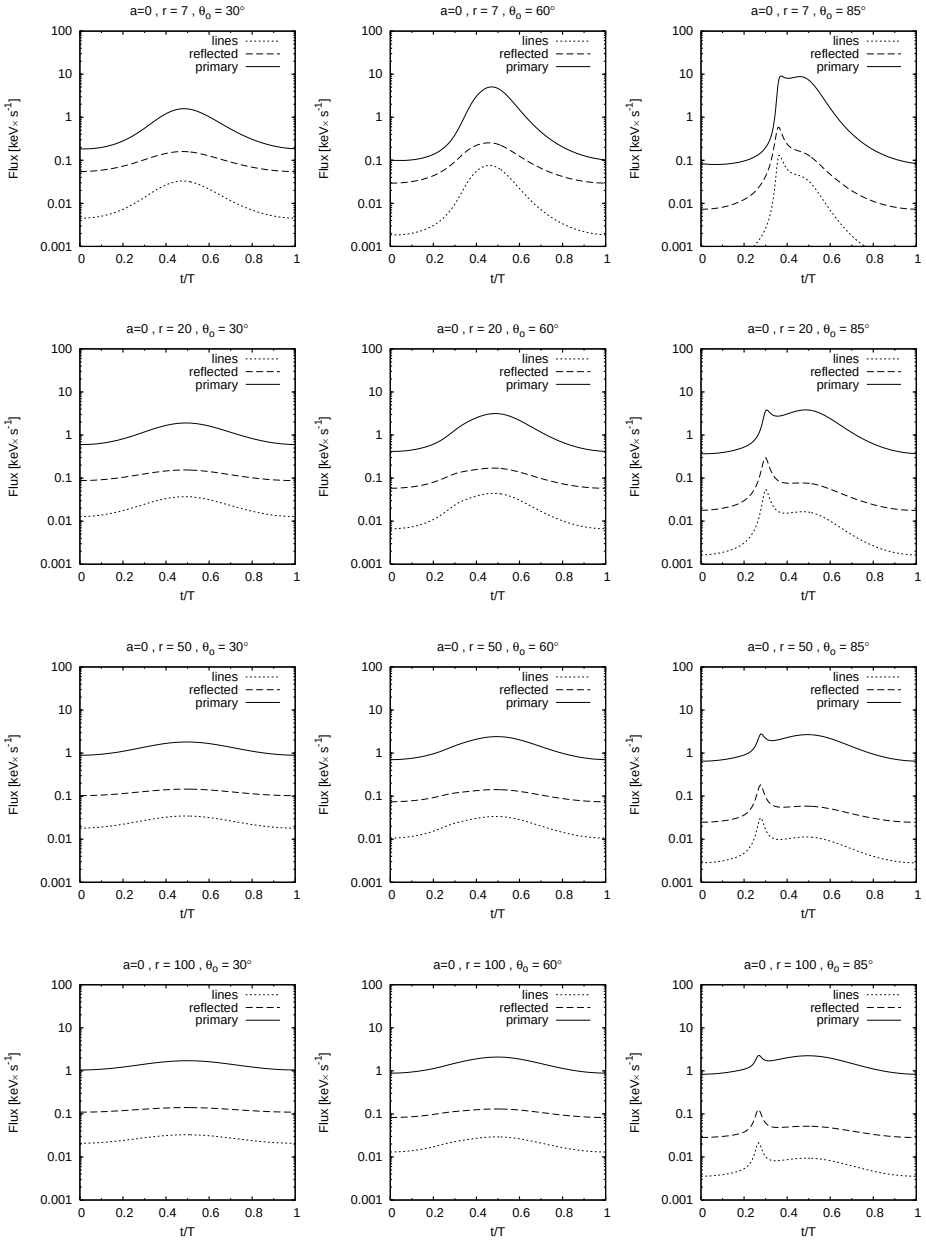

Figure 5. The same as in Fig. 4 but for the Schwarzschild black hole and the spot orbital radii 7, 20, 50 and 100 GM/c^2 (from top to bottom).

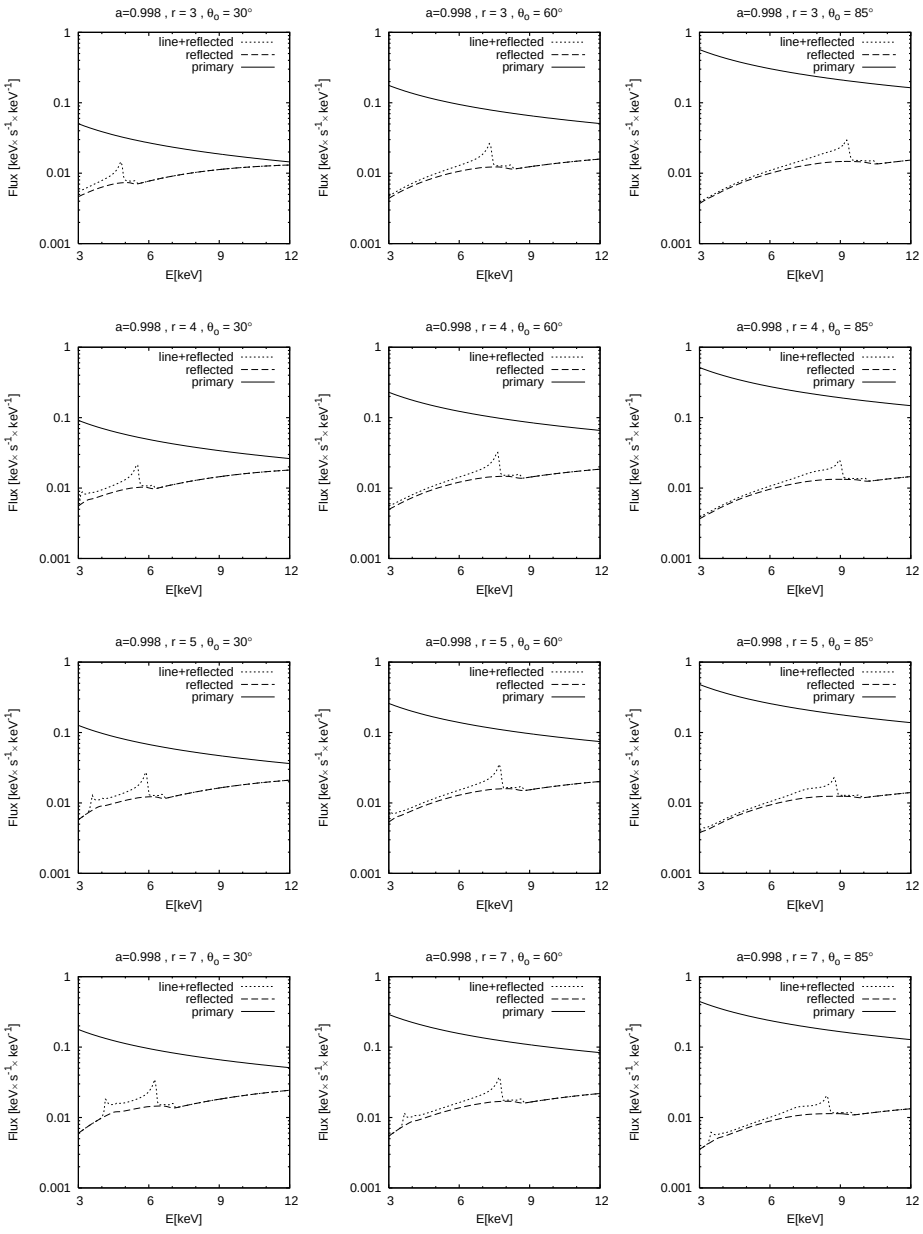

Figure 6. The observed spectra averaged over one orbit computed for the same set of parameters as in Fig. 4. Here, the observed line flux is shown on top of the spot continuum emission.

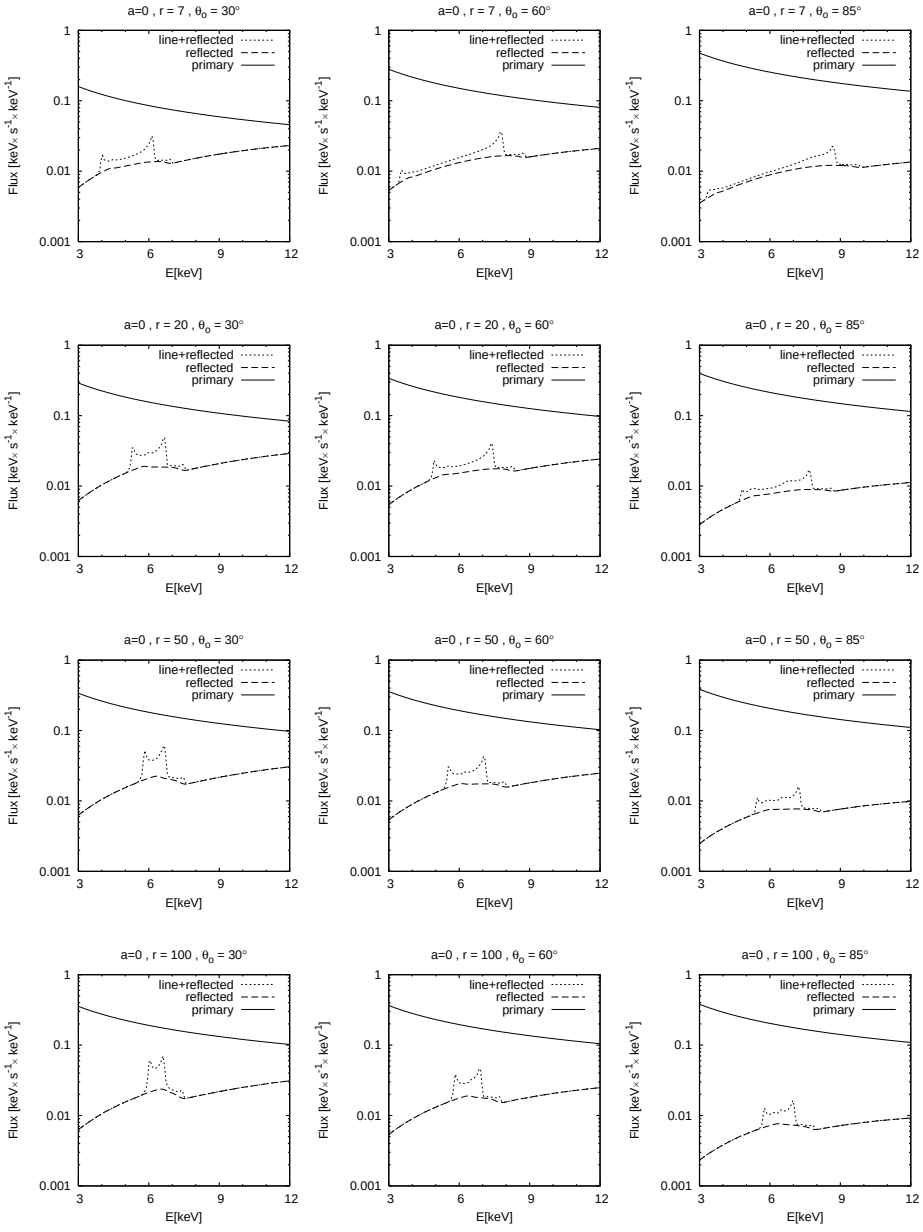

Figure 7. The observed spectra averaged over one orbit computed for the same set of parameters as in Fig. 5. Here, the observed line flux is shown on top of the spot continuum emission.

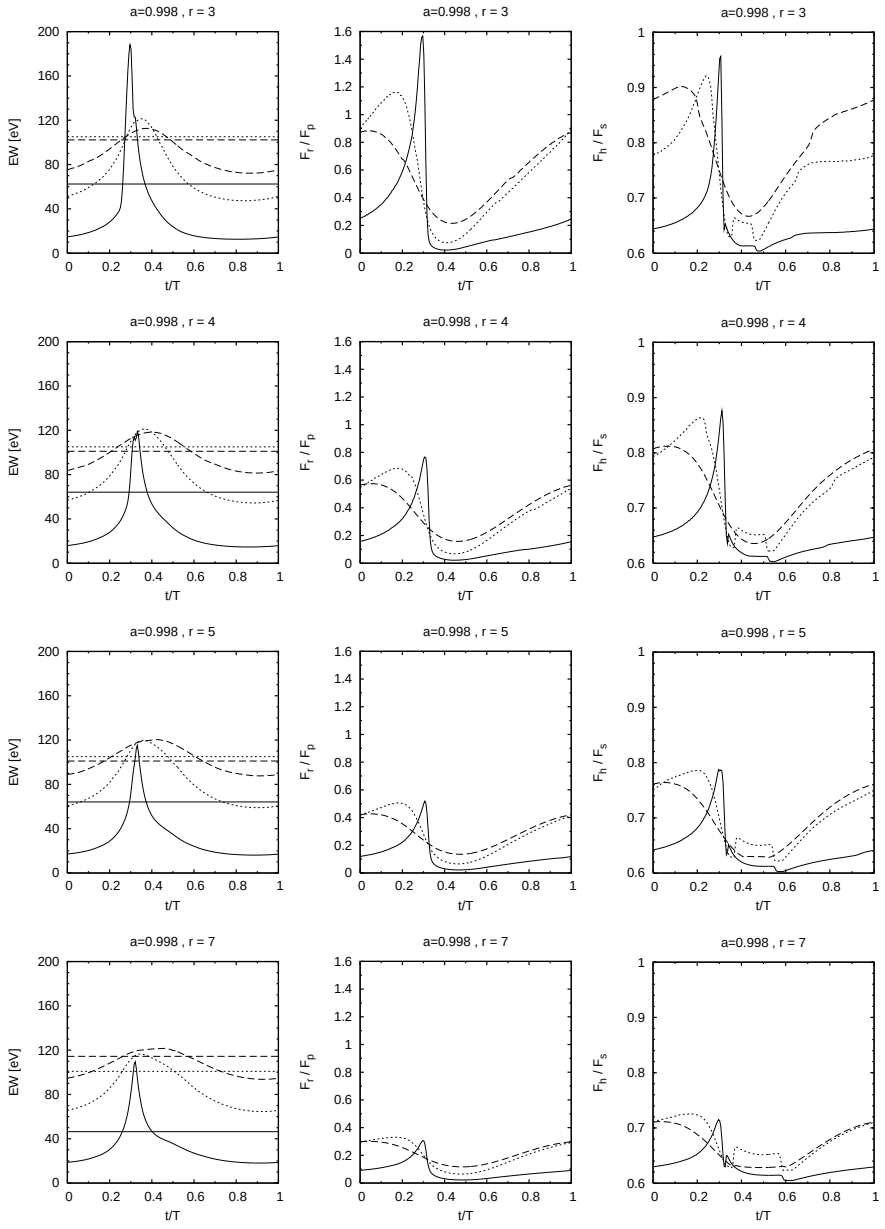

Figure 8. Left: The time variation of the observed EW of the Kα line. The integrated EW is shown in horizontal lines. **Middle:** The ratio of the observed reflected emission to the observed primary emission. The fluxes are integrated in the 3–10 keV energy range. **Right:** The hardness ratio of the hard flux $F_{\rm h}$ (6.5–10 keV) to the soft flux $F_{\rm s}$(3–6.5 keV). The flux in the Fe lines is also included. The dashed, dotted and solid lines correspond to the inclinations 30°, 60° and 85°.

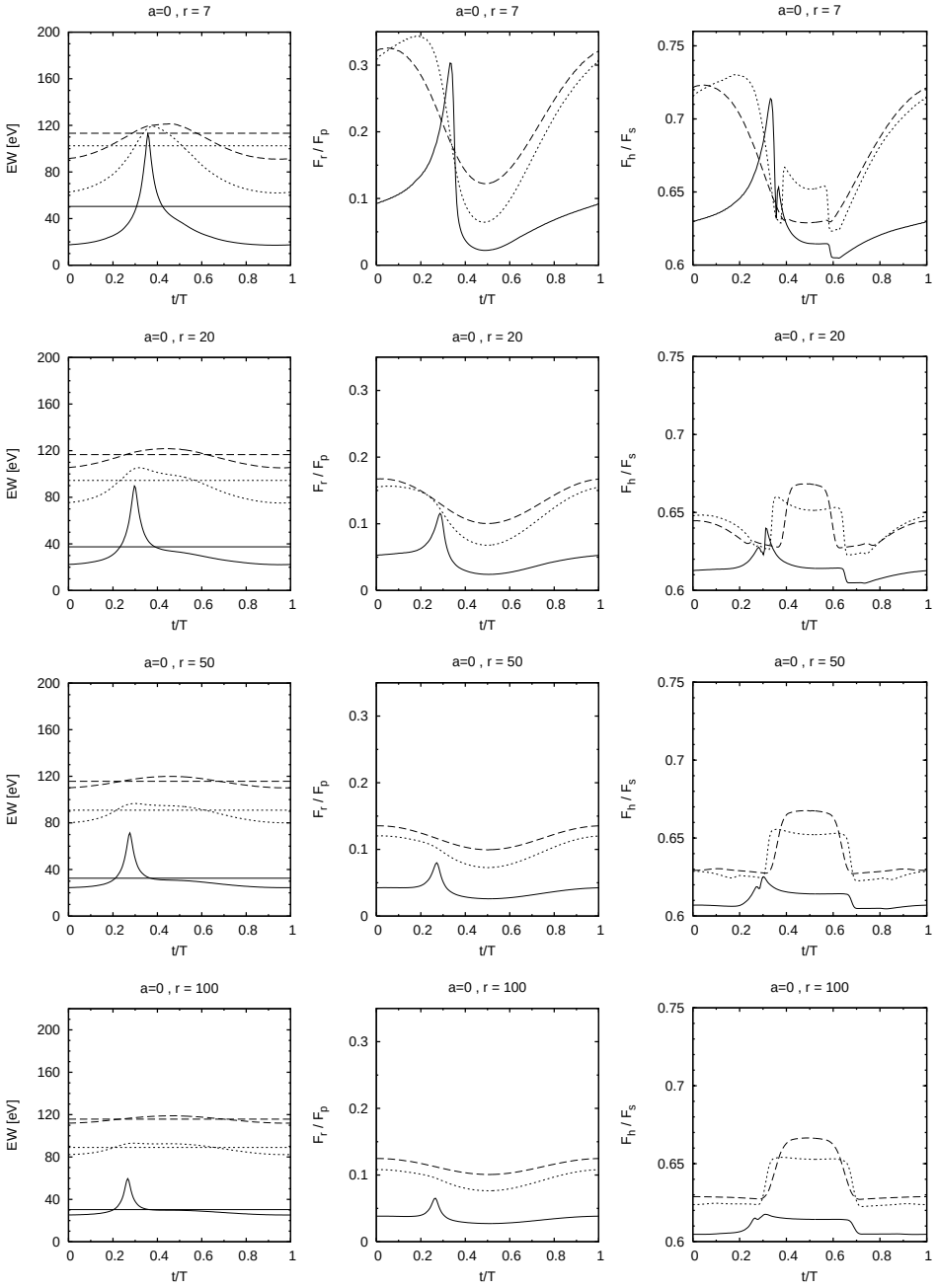

Figure 9. The same as in Fig. 8 but for the Schwarzschild black hole and the spot orbital radii 7, 20, 50 and 100 GM/c^2 (from top to bottom).

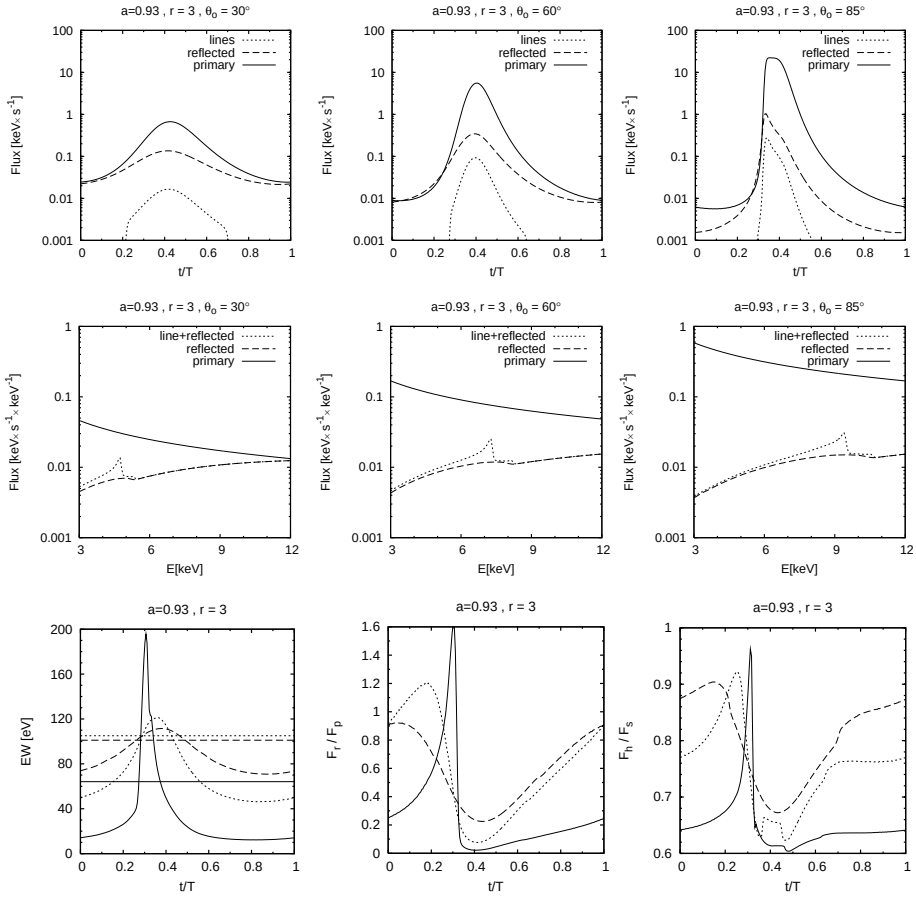

Figure 10. The same as in Figs. 4, 6, and 8 top rows (i.e. the spot orbital radius $3\,GM/c^2$) but for the Kerr black hole with the spin $0.93\,GM/c^3$.

as 200%. Similar to the flux variations at the larger radii the variation of the EW decreases. This is true also for all the other studied spectral characteristics.

The observed ratio of the reflected flux to the primary flux is amplified when compared to the local one, see the middle panels in Figs. 8 and 9 and the left panel in Fig. 3. The amplification is the highest for the lowest orbital radius and highest inclination angle — the ratio in this case is increased by more than one order of magnitude. Note that in the Kerr case with the orbital radius $3\,GM/c^2$ and for the inclinations 60° and 85° the ratio of the observed reflected flux to the observed primary flux is larger than unity, meaning the reflected component prevails over the primary one in a certain part of the orbit.

To evaluate the hardness ratio we compared the fluxes in between 3–6.5 keV (soft component, F_s) and 6.5–10 keV (hard component, F_h). The hardness ratio is also

amplified when we compare it with the local hardness ratio (the right panels in Figs. 8, 9 and 3). As in other spectral characteristics, the amplification and the variation of the hardness ratio is the largest for the lowest orbital radius in the extremally rotating Kerr case and they decrease with the increasing orbital radius.

To see how the different values of the spin parameter influence the studied properties of the observed signal we can compare the results for the same radius, see the bottom panels of Figs. 4, 6 and 8 for the extremally rotating Kerr black hole and compare them with the top panels of Figs. 5, 6 and 9 for the Schwarzschild black hole. For the closer radius, $r = 3\,GM/c^2$, we have computed the results for the spin $a = 0.93\,GM/c^3$ (the spin cannot be lower if the spot should be above the innermost stable circular orbit), see Fig. 10 and compare it with the top panels in Figs. 4, 6 and 8. It is clear from all of these comparisons that if we fix the orbital radius our results do not depend on the spin of the black hole.

4 CONCLUSIONS

We have studied the light curves, spectra and several spectral characteristics in the flare–spot model for different orbital radii of the flare. The primary flux was included and the mutual normalizations of the primary and reflected emission were treated within the framework of a simple, yet self-consistent scheme. About half of the isotropic primary flux hits the disc below the flare and is reprocessed there, creating a radiating spot. A part of the reprocessed radiation is re-emitted towards the observer. The radiation is influenced by the relativistic effects before reaching the observer.

We can sum up our results in several conclusions:

(1) The EW, apart for the extreme cases of high inclinations, does not differ significantly from the local EW. However, close to the black hole it varies even for low inclination of 30° by up to 30% when compared with its mean value for the whole orbit. The EW could be significantly amplified in our model only if the primary emission were beamed towards the disc, thus decreasing the observed primary emission.

(2) Both the ratio of the observed reflected to the observed primary flux and the hardness ratio are amplified when compared to the values for the intrinsic (local) emission.

(3) The variations of all of the studied spectral characteristics are the highest for close orbits and higher inclination angles.

(4) The spin of the black hole affects significantly our results only as far as it determines the location of the marginal stable orbit.

Here, we would like to remind the reader, that these results apply for a flare arising very near above the disc and thus they can heavily differ from the results of the light-bending model by Miniutti and Fabian (2004) where the flare orbits far above the disc and the resulting spot is much larger.

It follows from our results that the studied flux ratios could be used for estimating the lower limit of possible values of the spin parameter if the flare arises in the close vicinity of the black hole.

ACKNOWLEDGEMENTS

This research is supported by the ESA PECS project No. 98040. MD and VK gratefully acknowledge support from the Czech Science Foundation grants 205/05/P525 and 202/06/0041. GM acknowledges financial support from Agenzia Spaziale Italiana (ASI). RG is grateful for financial support to the Centre of Theoretical Astrophysics (LC06014).

REFERENCES

Collin, S., Coupé, S., Dumont, A.-M., Petrucci, P.-O. and Różańska, A. (2003), Evolution of the X-ray spectrum in the flare model of Active Galactic Nuclei, *Astronomy & Astrophysics*, **400**, pp. 437–449.

Dabrowski, Y. and Lasenby, A. N. (2001), Reflected iron line from a source above a Kerr black hole accretion disc, *Monthly Notices of the Royal Astron. Society*, **321**, pp. 605–614.

Dovčiak, M. (2004), *Radiation of Accretion Discs in Strong Gravity*, PhD Thesis, Charles University, Prague, arXiv:astro-ph/0411605.

Dovčiak, M., Karas, V., Matt, G. and Goosmann, R. W. (2007), Variation of the primary and reprocessed radiation from an orbiting spot around a black hole, *Monthly Notices of the Royal Astron. Society*, accepted.

Dumont, A.-M., Abrassart, A. and Collin, S. (2000), A code for optically thick and hot photoionized media, *Astronomy & Astrophysics*, **357**, pp. 823–838.

Fabian, A. C., Iwasawa, K., Reynolds, C. S. and Young, A. J. (2000), Broad Iron Lines in Active Galactic Nuclei, *Publications of the Astron. Society of the Pacific*, **112**, pp. 1145–1161.

Galeev, A. A., Rosner, R. and Vaiana, G. S. (1979), Structured coronae of accretion disks, *Astroph. Journal*, **229**, pp. 318–326.

George, I. M. and Fabian, A. C. (1991), X-ray reflection from cold matter in active galactic nuclei and X-ray binaries, *Monthly Notices of the Royal Astron. Society*, **249**, pp. 352–367.

Ghisellini, G., George, I. M., Fabian, A. C. and C., D. (1991), Anisotropic inverse Compton emission, *Monthly Notices of the Royal Astron. Society*, **248**, pp. 14–19.

Goosmann, R. W. (2006), *Accretion and Emission close to supermassive Black Holes in Quasars and AGN: Modeling the UV-X-spectrum*, PhD Thesis, Universität Hamburg, Germany.

Guainazzi, M. (2003), The history of the iron Kalpha line profile in the Piccinotti AGN ESO 198-G24, *Astronomy & Astrophysics*, **401**, pp. 903–910.

Iwasawa, K., Fabian, A. C., Reynolds, C. S., Nandra, K., Otani, C., Inoue, H., Hayashida, K., Brandt, W. N., T.Dotani, Kunieda, H., Matsuoka, M. and Tanaka, Y. (1996), The

variable iron K emission line in MCG-6-30-15, *Monthly Notices of the Royal Astron. Society*, **282**, pp. 1038–1048.

Martocchia, A., Karas, V. and Matt, G. (2000), Effects of Kerr space-time on spectral features from X-ray illuminated accretion discs, *Monthly Notices of the Royal Astron. Society*, **312**, pp. 817–826.

Martocchia, A. and Matt, G. (1996), Iron Kalpha line intensity from accretion discs around rotating black holes, *Monthly Notices of the Royal Astron. Society*, **282**, pp. L53–L57.

Matt, G., Fabian, A. C. and Ross, R. R. (1993), Iron K-alpha lines from X-ray photoionized accretion discs, *Monthly Notices of the Royal Astron. Society*, **262**, pp. 179–186.

Merloni, A. and Fabian, A. C. (2001), Accretion disc coronae as magnetic reservoirs, *Monthly Notices of the Royal Astron. Society*, **321**, pp. 549–552.

Miniutti, G. and Fabian, A. C. (2004), A light bending model for the X-ray temporal and spectral properties of accreting black holes, *Monthly Notices of the Royal Astron. Society*, **349**, pp. 1435–1448.

Miniutti, G., Fabian, A. C., Goyder, R. and Lasenby, A. N. (2003), The lack of variability of the iron line in MCG-6-30-15: general relativistic effects, *Monthly Notices of the Royal Astron. Society*, **344**, pp. L22–L26.

Misner, C. W., Thorne, K. S. and Wheeler, J. A. (1973), *Gravitation*, Freeman, San Francisco.

Niedzwiecki, A. and Zycki, P. T. (2007), On variability and spectral distortion of the fluorescent iron lines from black-hole accretion discs, *Monthly Notices of the Royal Astron. Society*.

Poutanen, J. and Fabian, A. C. (1999), Spectral evolution of magnetic flares and time lags in accreting black hole sources, *Monthly Notices of the Royal Astron. Society*, **306**, pp. L31–L37.

Reynolds, C. S. and Nowak, M. A. (2003), Fluorescent iron lines as a probe of astrophysical black hole systems, *Phys. Reports*, **377**, pp. 389–466.

Turner, T. J., Mushotzky, R. F., Yaqoob, T., George, I. M., Snowden, S. L., Netzer, H., Kraemer, S. B., Nandra, K. and Chelouche, D. (2002), Narrow Components within the Fe K Profile of NGC 3516: Evidence of the Importance of General Relativistic Effects?, *Astroph. Journal*, **574**, pp. L123–L127.

Yaqoob, T., George, I. M., Kallman, T. R., Padmanabhan, U., Weaver, K. A. and Turner, T. J. (2003), Fe XXV and Fe XXVI Diagnostics of the Black Hole and Accretion Disk in Active Galaxies: Chandra Time-resolved Grating Spectroscopy of NGC 7314, *Astroph. Journal*, **596**, pp. 85–104.